Characterisation and Integration of Piezoelectric Trimorph Actuators for Blade Active Surface Control on a Scaled Wind Turbine

Journal of Physics: Conference Series **2767** (2024) 092094 doi:10.1088/1742-6596/2767/9/092094

Characterisation and Integration of Piezoelectric Trimorph Actuators for Blade Active Surface Control on a Scaled Wind Turbine

J P Fuentes Holden[1,2], L Gan[1], D Sims-Williams[1], J Gilbert[2], P Osborne[3] and M Bastankhah[1]

[1] Department of Engineering, Durham University, Durham, DH1 3LE, UK
[2] Aura CDT in Offshore Wind Energy and the Environment, University of Hull, UK
[3] University of Sheffield, Sheffield, South Yorkshire, UK

Email: jordan.p.fuentes-holden@durham.ac.uk

Abstract. The paper investigates the integration of piezoelectric bending actuators on trailing edge flaps (TEF). The characterisation of piezoelectric actuators is of great importance due to differences in performance resulting from sample variability, actuator construction, circuit type and equipment. For the application of trailing edge flaps in scaled turbines, the total deflection these actuators can produce determines the possible flap angles and, consequently, the potential effects on wake evolution downwind of the wind turbine. In this paper, we fully characterise the performance of the piezoelectric bending actuator under a variety of operating conditions. The bridged bi-polar circuit is used to drive the piezoelectric actuators with both a static and a dynamic signal. Deflection results demonstrate that the piezoelectric actuator is capable of achieving flap angles of $\beta \pm 3°$ with a static signal, and $\beta = 2.3°$ and $\beta = -3.2°$ angles with a dynamic signal. Experimental force measurements using a dynamic signal result in a force reduction of up to 33% when compared to a static signal. Force values at increasing frequencies do not show a depreciation in force. Additionally, initial aerodynamic loads exerted on TEF are presented based on XFoil simulations to ensure that the piezoelectric actuating force can overcome aerodynamic loads for future experiments. Experimental force measurements from the piezoelectric actuator demonstrate that aerodynamic forces can be overcome. This work serves as the first step towards implementing the TEF technology in lab-scaled wind turbine models.

Keywords: Offshore wind, wind turbines, trailing edge flaps, piezoelectric actuators

1. Introduction

Wind turbines (WT) have been increasing steadily in size due to the economies of scale [17, 22]. However, upsizing a WT brings increased structural challenges, particularly when it comes to aerodynamic loading on the rotor. Unsteady factors such as WT wakes and wind shear are exacerbated and affect the operational stability of WTs. Moreover, the blades start to experience larger flow variations over their span. A technology proposed to mitigate this problem is called 'smart rotor control' [3, 5, 13]. This involves installing local distributed aerodynamic active control systems with built-in intelligence along the blades. These aerodynamic control surfaces include trailing edge flaps, microtabs and boundary layer control methods like synthetic jets or plasma actuators. These are coupled with actuators, controllers and sensors to form the smart rotor control system. Barlas and van Kuik [3], and Awada *et al* [1] provide a comprehensive review on these technologies. The most researched and promising are TEFs.

TEFs function by modifying the aerofoils camber line, an increased camber results in an increase in lift, whereas a decrease camber results in lower lift values [9]. Two types of TEF mechanisms exist, one is the discrete flap (hinged type) and the other is the adaptive trailing edge geometry (morphing type). It has been shown that when the flap-to-chord ratio (f/c) is 0.1-0.15 (i.e. the flap occupies 10-15% of the aerofoil chord), a 1° change in the flap angle produces an equivalent lift change as a 0.5° pitch adjustment of the entire airfoil section [13]. This shows that even with small surface deflections of the TEF, significant change in lift can be achieved over the entire blade. Additionally, due to their much lower inertia, the power requirement to operate these devices is much smaller than partial or full span pitch control. This also means that high frequency control is possible, which is important for mitigating loads in the high frequency load spectrum. Various studies have demonstrated the benefits of this technology from lab-scale demonstrators, field-studies and retrofitting of full scale WTs [4, 6, 8, 10, 12].

Numerous actuation methods have been proposed to enable movement of TEFs. These vary based on their application, particularly when it comes to weight requirements and broadband response. Smart materials such as shape memory alloys (SMA) and piezoelectric actuators have been a popular choice for TEFs due to large energy to weight ratios and fast actuation when compared to traditional actuators based on pneumatics or hydraulics [3]. Piezoelectric actuators come in a variety of forms, but for TEF devices, macro-fibre composites (MFC) or piezoelectric benders are commonly used. These actuators have been particularly useful for enabling TEFs in experimental scaled-down models of wind turbine and helicopter research. MFCs are composed of piezoelectric fibres embedded in a polymer matrix. This allows them to be flexible and highly conformable to most shapes like aerofoil surfaces. They provide large deflections but require high voltages ($> 1\,\text{kV}$) for operation [7]. On the other hand, piezoelectric benders are rigid and provide smaller deflections but require much smaller voltages to operate.

In a study by Bilgen *et al* [7], MFCs are used to actuate the TEF from a 2D aerofoil. The MFCs are bonded to the pressure and suction side of the aerofoil. A compliant single four-bar (box spar) mechanism as the internal structure allows for an adaptable trailing edge geometry. The f/c for this model is ≈ 0.72 and the flap angles achieved are over $\pm 10°$. In this study, wind tunnel experimental measurements are conducted to identify the hysteresis effect of the piezoelectric MFCs on the TEF displacement when aerodynamically loaded. The lift-to-drag ratio C_L/C_D at low Reynolds chord Re_c numbers (1-1.5 $\times 10^5$) is calculated and the performance is shown to be comparable to a NACA 0009 aerofoil tested by Selig [23].

Bak *et al* [2] used piezoelectric benders to actuate the TEF from a 2D aerofoil model. The TEF occupies the entire span of the model and has a f/c of ≈ 0.1 with a range of flap angles of $\approx \pm 2°$. The study tested static and dynamic operating modes of the bender and its efficacy in cancelling induced loads from a sinusoidal pitching motion by measuring the change in lift coefficient ΔC_L. It was found that the TEF could reduce the amplitude by up to 80%. Later, a follow-up study by van Wingerten *et al* [24] also used piezoelectric benders to actuate TEFs on a 2D aerofoil model. This time, there are two TEF devices through its span and have a $f/c = 0.5$. Similarly, a sinusoidal pitching motion is used to simulate the 1 and 3P disturbances experienced on wind turbines. For this experiment, the TEF is actuating at a phase difference of 8° of the pitching frequency and the piezoelectric bender is deflecting due to a dynamic signal amplitude of ±400V which led to a 90% reduction in strain. Lastly, a study by Hulskamp *et al* [14] utilised once again piezoelectric benders for actuating the TEFs from a scaled down wind turbine. The WT featured two blades, each equipped with two TEFs. These are placed as far outboard as possible and have a $f/c = 0.6$. As with the previous studies [2, 24], the objective was to attenuate the blades vibrations through aerodynamic dampening.

It is to the authors knowledge that the application of TEF technology has been strictly focused on load mitigation strategies or power conversion efficiency in WTs. However, just like pitching and yaw control methods found in WTs [19], TEFs could potentially be used for other strategies such as WT wake mitigation. The following paper aims to take the initial steps on developing a TEF system using piezoelectric bending actuators for integration into a scaled model WT. To begin, a 2D aerodynamic parametric study is carried out to estimate the aerodynamic loads on the TEFs. This is then followed by the characterisation of a piezoelectric actuator through experimental methods. The study aims to bring clarity of driving mechanisms of the piezoelectric bending actuators and other factors to consider. Understanding the control mechanisms and characteristics of the piezoelectric actuator will serve as one of the building blocks for future works investigating the impact of TEFs on WT wakes.

2. Piezoelectric Bending Actuator: Nomenclature and Basic Definition

Piezoelectric benders (otherwise known as piezos) are generally used in a cantilever arrangement [20]. They are available in several configurations, however for this study, a piezoelectric trimorph bender is used. This piezo bender has a double layer of active piezos with a passive substrate layer in the middle [16]. Figure 1 shows a schematic of the piezoelectric trimorph actuator with outwards polarisation. An important feature of the piezo is the maximum achievable peak-to-peak tip deflection δ_{p-p} relative to its free length L_{free}. This is important because a greater δ results in a larger flap angle. The fixed length L_{Fixed} does not deflect and this is where connections and mounting are performed. The blocking force F_{blk} is measured as the force required to return from its maximum displacement to its neutral position [16].

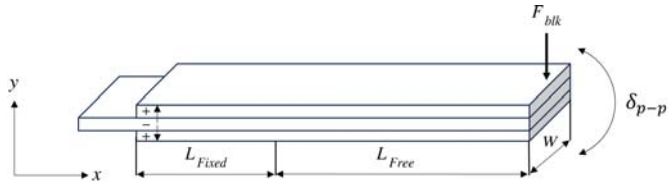

Figure 1: Schematic of piezoelectric trimorph actuator adapted from [20].

A full characterization of the piezoelectric actuators is critical due to the known performance variability from sample to sample, piezo construction and electrical configuration. Therefore, each individual actuator must undergo testing, particularly if we aim to use multiple actuators in one single flap. Moreover, in-situ measurements of the TEF angle on wind turbine blades is extremely challenging due to the high rotational speed of the rotor and the associated blade bending motions. Hence, the objective of our work is to develop a precursor experimental setup (outside the wind-tunnel) capable of systematically characterising the performance of piezoelectric actuators before conducting wind-tunnel experiments. The data obtained from the precursor experiments will be compiled into a look-up table. This table will facilitate determining the achieved flap angle for turbine blades in real-time accounting for all relevant factors such as input electrical voltage, hysteresis, drift effects, and external forces.

3. TEF Aerodynamic Performance

Scaled-down model WTs inevitably have a Re_c mismatch due to their much smaller chord length. A full scale WT will operate at $Re_c > 10^6$, whilst a scaled-down model WT may operate at $Re_c < 10^5$. Because of this, the RG-14 aerofoil was selected due to its good performance at low Re_c numbers as demonstrated in a study by Nanos et al [18]. The geometrical features of the RG-14 can be seen in Figure 2(a). Additionally, the flap angle β definition can be seen in Figure 2(b). This is the angle produced by the TEF when actuated with respect to the aerofoil chord length c and the hinge position from the flap length f.

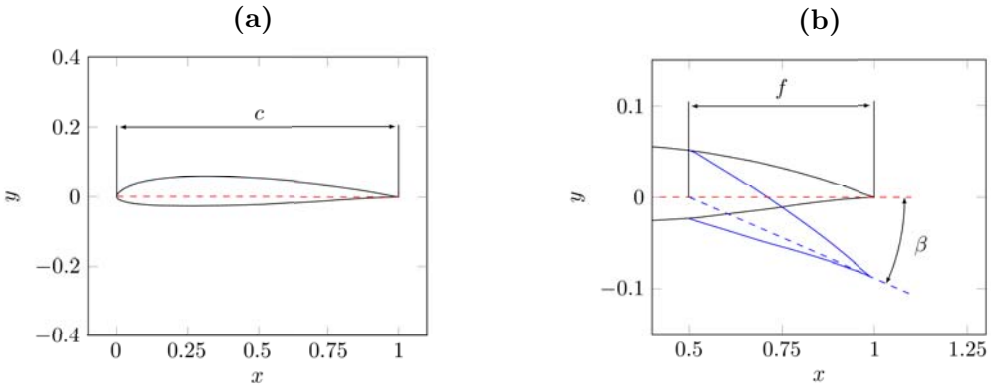

Figure 2: **(a)** RG-14 aerofoil geometry and **(b)** TEF flap angle β definition.

The flap performance is investigated using 2D XFoil simulations. Using a parametric analysis, we investigate the impact of different flap angles β and flap-to-chord ratios f/c on the aerodynamic performance of the RG-14 aerofoil at $Re_c = 10^5$. Figure 3 shows the variations of the C_L and the C_L/C_D with angle of attack α. Data from $\beta = 0$ (Exp) indicates the experimental polars of the RG-14 aerofoil obtained from an experimental study by Selig [23] operating at a $Re_c = 10^5$. When compared to the XFoil simulation at $\beta = 0°$, overall reasonable agreement is shown. The other cases have a flap angle of $\beta \pm 2°$. This angle is used based on the achievable deflection from the piezoelectric bender, which will be discussed later in detail. Figure 3(a) shows that a positive flap angle (increase in camber) results in an increase in C_L, whilst a negative flap angle results in a drop at all angles of attack. Moreover, as shown in Figure 3(b), the flap-to-chord ratio has an important effect on the aerofoil performance. A flap-to-chord ratio of $f/c = 0.7$ results in higher values of C_L and C_L/C_D, especially at low angles of attack, compared to cases with $f/c = 0.5$ and 0.2.

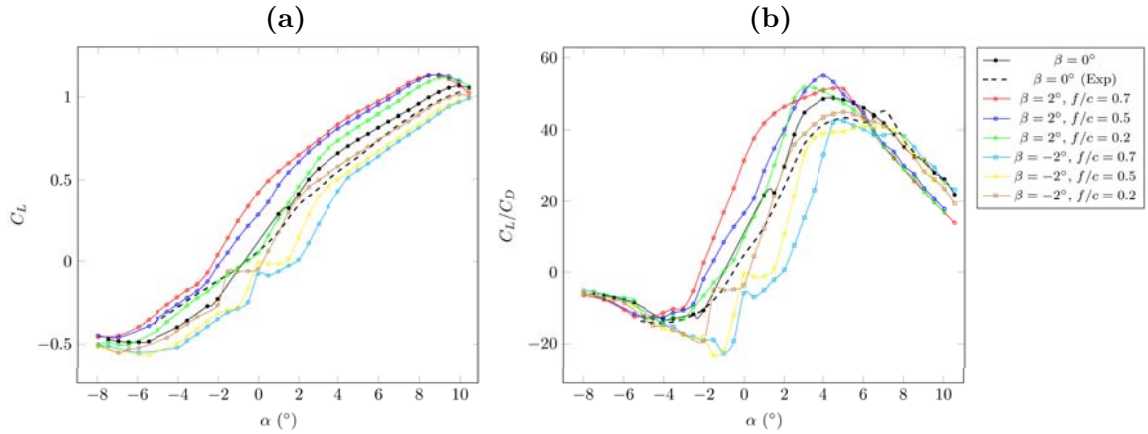

Figure 3: XFoil simulations on RG-14 aerofoil with TEF. For comparison, the experimental data from [23] is shown for $\beta = 0°$. Effect of flap angle ($\pm 2°$) and flap-to-chord ratio f/c on **(a)** lift coefficient C_L and **(b)** lift-to-drag ratio C_L/C_D.

3.1. TEF Aerodynamic Load Estimations

To ensure the applicability of the results obtained from our precursor simulations to future WT experiments, we need to verify that the aerodynamic loads exerted on the TEF are fairly small and cannot affect the deflection δ of the actuators. To do so, we compare aerodynamic forces with the actuating force of the piezoelectric bender. This is done based on the results from XFoil simulations discussed earlier. The main force the piezoelectric bender must overcome is the lift force F_L. The largest F_L occurs when C_L is at its maximum value, which can be seen in Figure 3(a). We define this operating point as $C_{L,max}$, which happens at specific angles of attack. One can also observe from Figure 3(a) that the largest $C_{L,max}$ values occur when $\beta = 2°$. Thus calculations are only performed only for these cases. The local lift coefficient $C_{L,local}$ for the flap section of the aerofoil is computed by integrating the pressure coefficients along the flap surface.

The results found on Table 1 show the lift coefficients for both the entire aerofoil and the flap, as well as the local lift force, given by the following expression,

$$F_{L,local} = 0.5\rho C_{L,local} u_{rel}^2 A_p, \tag{1}$$

where $\rho = 1.204\,\mathrm{kg/m^{-3}}$ is the air density at 20°C, $u_{rel} = 25\ \mathrm{ms^{-1}}$ is relative wind speed and A_p is the planform area of the TEF. The span of the flap measures 30 mm and the aerofoil chord is 60 mm. Results show that the highest loading is found to be for the flap located at $f/c = 0.7$ and as expected, aerodynamic loads decrease with a decrease of f/c. It is important to note that our analysis here tends to overestimate aerodynamic loads because we use a conservative estimation with high angles of attack. Nonetheless, in the next section, it will be shown that the F_{blk} for the chosen piezoelectric actuator is still greater than these conservative aerodynamic estimates.

Table 1: Estimation of the maximum aerodynamic loading on TEF.

α (°)	f/c	β (°)	$C_{L,max}$	C_D	$C_{L,local}$	$F_{L,local}$ (N)
8.5	0.2	2	1.106	0.038	0.363	0.05
9.5	0.5		1.106	0.054	0.614	0.21
8.5	0.7		1.124	0.044	0.819	0.39

4. Detailed Characterisation of Piezoelectric Actuators

4.1. Electrical Circuit

Piezoelectric bending actuators usually trade-off force for a large displacement [11]. Thus it is important to quantify the F_{blk} to ensure it can overcome the $F_{L,local}$. The chosen piezoelectric trimorph actuator was provided by Hoerbiger and their Type 5 variant was used. The actuator is manufactured using carbon fibre coating technique. Some of the datasheet properties of the piezoelectric actuator can be found in Table 2, where the given δ_{p-p} and F_{blk} is obtained at ± 230 V.

Table 2: Piezoelectric trimorph actuator properties.

L_{Free} (mm)	L_{Fixed} (mm)	Width, W (mm)	δ_{p-p} (mm)	F_{blk} (N)
38	9	5.9	2.8	0.45

To drive the piezoelectric actuator, a driver called BD300 by PiezoDrive was used. This driver provides amplification and dual channelling option with an inverter switch that allows the piezoelectric actuator to be driven differentially. The type of circuit used is known as the bridged bi-polar [20]. It requires only two wires to drive the piezoelectric actuator since its polarisation is outwards, where each wire is connected to a piezoelectric layer. This circuit can be seen in Figure 4.

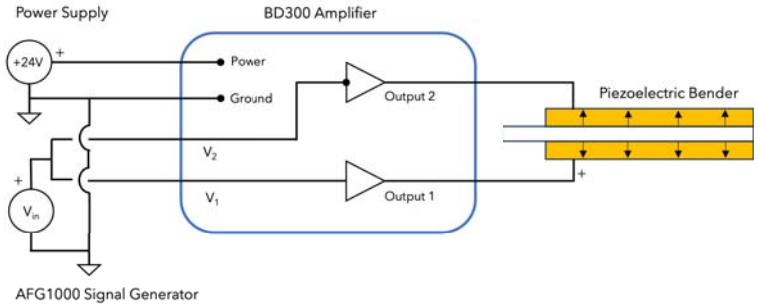

Figure 4: Piezoelectric actuator bridged bipolar circuit.

Two types of input signals V_{in} were tested, a constant DC voltage and a sinusoidal waveform. These were generated by a AFG1000 signal generator from Tektronix. The voltages generated ranged from 0 to 3 V and these were amplified to a range ± 300 V. The voltage across the bottom piezo (V_1) layer is given by the expression in equation 2, where $K = 101$ is the amplifier gain. On the other hand, the inverted signal (V_2) gives the expression shown in equation 3. The value 1.5 in the equation is the voltage offset.

$$V_1 = KV_{in} \quad (2) \qquad V_2 = 2K(V_{in} - 1.5) \quad (3)$$

4.2. Experimental Set-up

To measure the deflection produced by the piezo, a laser displacement sensor ILD 1220-50 by Micro-Epsilon was used. The laser has a resolution of 1 μm and a sampling rate of 1 kHz, enabling full capture of the piezo's deflection range. The laser works by the triangulation method, where the diffuse reflection from the target surface (i.e. the piezo) is detected by a CMOS sensor. The laser dot is carefully aligned to be as close to the tip of the actuator as possible. The experimental set-up is shown in Figure 5(a). For measuring the piezo's F_{blk}, an FSS1500NST sensor by Honeywell is used. The experimental set-up for measuring the piezo actuation force can be seen in Figure 5(b). A similar arrangement is used in studies by [20, 21]. For both set-ups, data is recorded using a data acquisition (DAQ) device from National Instruments (USB-6003). The DAQ features a 16-bit resolution and a maximum sampling rate of 100 kS/s. Measurement controls and visualisation of both systems are conducted in LabVIEW software.

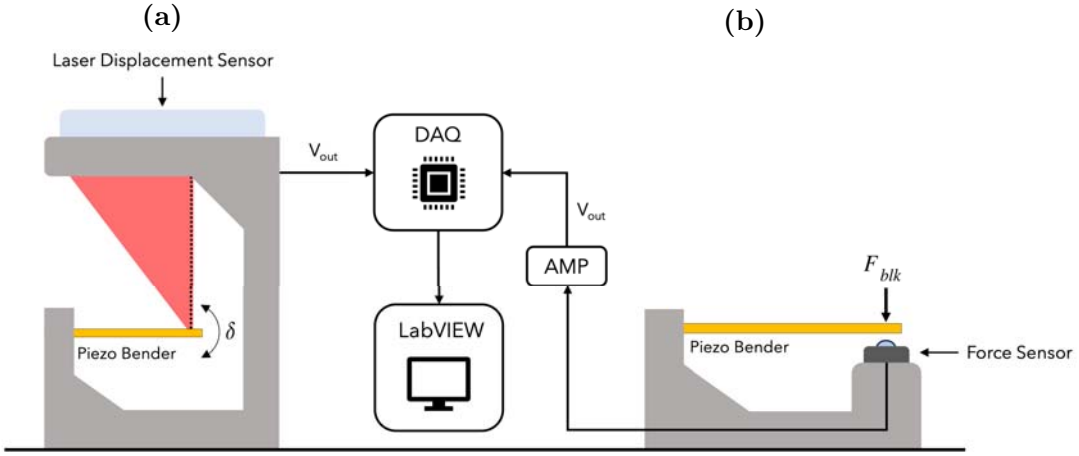

Figure 5: Experimental set-up for measuring piezoelectric bender **(a)** deflection and **(b)** force.

4.3. Deflection Performance Characterisation

The deflection performance of the piezoelectric benders is important since this determines the possible flap angles. This section includes a series of deflection experiments. Firstly, four piezo benders are compared using a dynamic signal and thereafter, three other experiments are conducted using a single piezo. These three experiments are: a dynamic signal with amplitude variation at a fixed frequency, a dynamic signal with frequency variation at a fixed amplitude and lastly, a test using static DC voltage signals.

For the input voltage V_{in}, a dynamic sinusoidal waveform signal is used with a peak-to-peak voltage $V_{p-p} = 3\,\text{V}$ at a frequency of 1 Hz. These conditions are similarly employed in a study performed by Rios [20]. This comparison is performed in order to address sample variability and repeatability. The δ_{p-p} as well as the V_{in} can be seen in Figure 6(a). For each piezo, the zero value is set to the middle of the δ_{p-p} for comparison reasons. Here, the difference between the largest δ_{p-p} and the smallest is 8%. Furthermore, the upper sweep ($V_{in} = 0 \rightarrow 3\,\text{V}$) and the lower sweep ($V_{in} = 3 \rightarrow 0\,\text{V}$), shows similarity between all four in a 5 minute test run. Error bars are present in this graph, albeit barely visible due to its excellent repeatability.

The next test investigates V_{p-p} variation with a constant signal frequency at 1 Hz. For a single piezo, shown in Figure 6(b), the flap angle β is used instead of δ for the corresponding V_{in}. This is done since β provides a more meaningful value for TEF performance than δ. Results on Figure 6(b) show that increasing V_{p-p} from 1 to 3.5 V increases the flap angles by up to 425%. This is expected as there is an increase in electric field strength. At 3.5 V_{p-p}, the voltage limits ($\pm$ 300 V) of the amplifier are exceeded, there is a clear biasing direction towards negative β values and both β peaks plateau. Furthermore, there is an increase in expansion and separation between the upper and lower sweep, known as the hysteresis effect. The hysteresis effect is a known issue in piezoelectric actuators [3, 20], where the displacement is not only determined by the current input voltage, but also the historical input voltage. The displacement of a piezoelectric actuator is caused by the electrostrictive, inverse

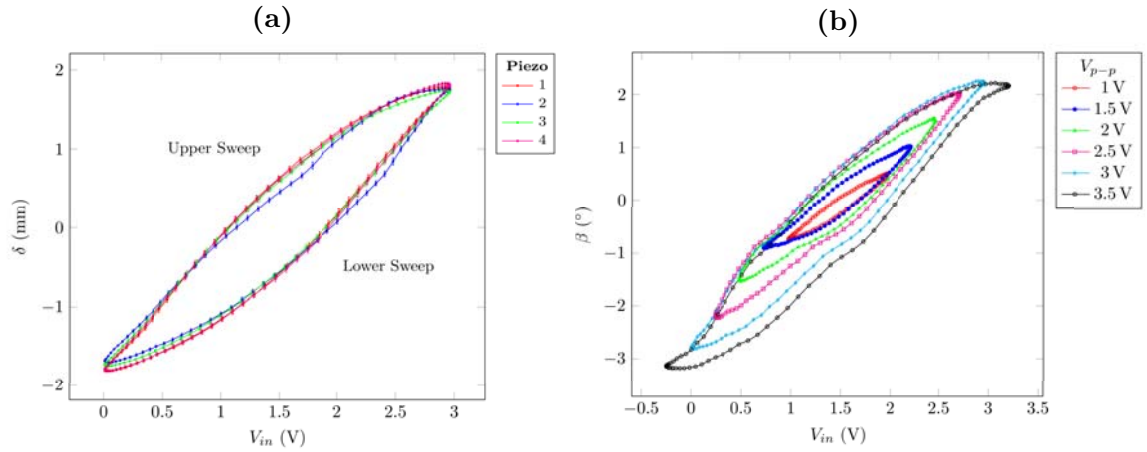

Figure 6: Piezoelectric bender deflection driven with a dynamic signal. **(a)** Comparison of four selected piezos at $3V_{p-p}$ and 1 Hz. **(b)** Variation of V_{p-p} at 1 Hz.

piezoelectric and ferroelectric effect. Li *et al* [15] suggested that the main driver of hysteresis is the ferroelectric effect, specifically the partially irreversible non-180° domain steering.

The last dynamic signal test involved varying the signal frequency from 1 to 50 Hz. The V_{p-p} is kept at 3 V. Results from Figure 7(a) show that an increase in frequency leads to a decrease in flap angles and an increase in hysteresis. It is believed that the main driver of this increase in hysteresis is due to the low slew rate of the amplifier. Bak *et al* [2] also experienced this limitation in their study with piezoelectric benders. The slew rate, dictates how fast a piezo can be charged and discharged, it is given by

$$Slew\ rate = \frac{dV}{dt} = \frac{I_{max}}{C}, \tag{4}$$

where I_{max} is the maximum delivered current by the piezo driver, and C is the piezoelectric actuators capacitance.

In Figure 7(b), a DC input voltage V_{in} is used and the piezo deflection is measured over a period of 9 minutes. It is possible to notice that the voltages used fall outside the operational limit of the amplifier (-0.5 and 3.5 V) and the achievable flap angles are greater than when driven with a dynamic signal. At 1.5 V (i.e. the voltage offset), the piezo should remain undeflected and at $\beta \approx 0°$. However, hysteresis is observed when returning to some 1.5 V values since $\beta \not\approx 0°$. This is a known behaviour of piezoelectric actuators when they are deflected to their limits and afterwards they remain partially charged. Similar behaviour is seen with the MFCs used in the study by Bilgen *et al* [7]. Lastly, drifting of β over time is also seen for almost all changes in voltage.

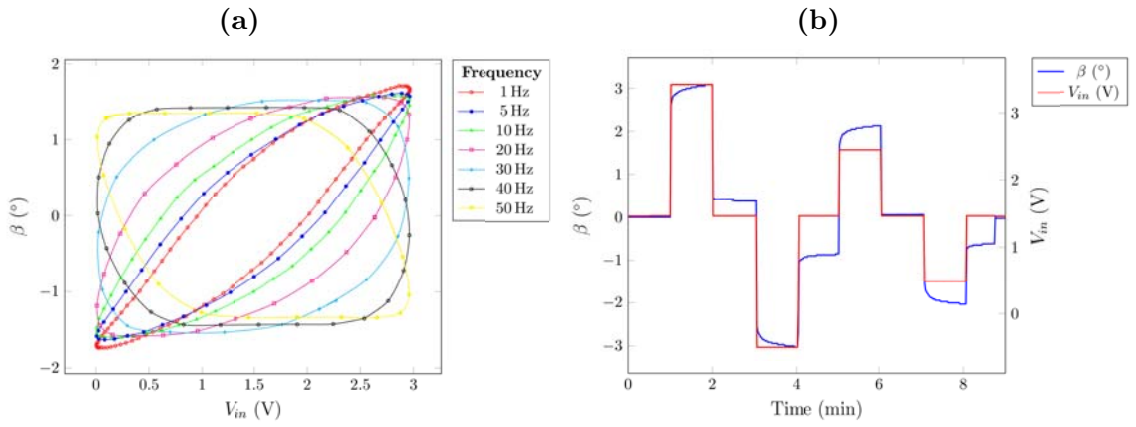

Figure 7: Piezoelectric bender actuator deflection measurements using **a)** dynamic signal with frequency variation at $3V_{p-p}$ and **b)** static DC voltage signals.

Overall, when using a dynamic signal the piezoelectric benders prove to be similar from the four piezos compared. Additionally, the standard error values are small and no drifting is observed. It is also shown that the deflection is repeatable over a range of V_{p-p} at 1 Hz. However, hysteresis effect is significant when driven at increasing frequencies. On the other hand, static DC voltage signals demonstrate larger flap angles than with a dynamic signal but present some drifting and less predictable hysteresis effect.

4.4. Force Performance Characterisation

Experimental force measurements are necessary to ensure the piezoelectric bender can overcome aerodynamic forces for future experiments. Just as the deflection measurements, the same types of signal are tested. In Figure 8(a) static DC voltage signals are used from 1.5 to −0.5 V at decreasing intervals of 0.5 V over a period of 7 minutes. As expected, the blocking force F_{blk} increases as the piezo is deflected further downwards. At each interval, drifting is observed just as the static deflection measurements shown in Figure 7(b). The maximum F_{blk} is 0.52 N at −0.5 V. In Figure 8(b), a dynamic sinusoidal signal is used to measure F_{blk} with frequency of 0 to 30 Hz and $3V_{p-p}$. Each data point shown is the averaged peak force measurement taken over a one minute test period. The highest measured F_{blk} = 0.41 N and is obtained at a frequency of 0.5 Hz. The F_{blk} decreases to 0.37 N at 1 Hz and fluctuates with increasing frequency. The smallest recorded F_{blk} is 0.35 N, which is found at 15 and 20 Hz. Both recorded force measurements differ from the F_{blk} value on the manufacturers data sheet (see Table 2), static DC voltage signals produce a higher than expected F_{blk} and dynamic signals less than expected. This is likely due to differences in electrical circuit, operating conditions and experimental set-up.

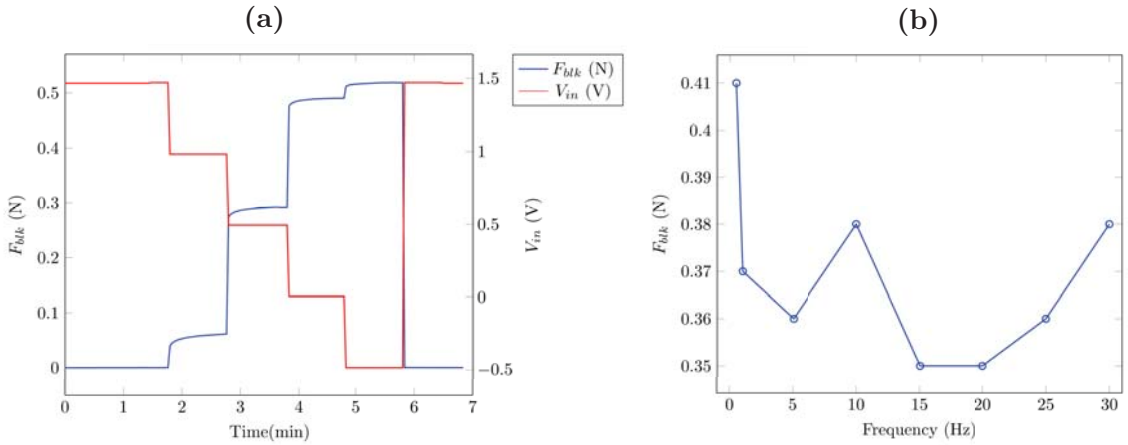

Figure 8: Piezoelectric bender actuator force measurements using **a)** static DC voltage signals and **b)** dynamic voltage signals at varying frequencies at $3V_{p-p}$.

As previously demonstrated in Section 3.1, the estimated maximum aerodynamic load exerted on the TEF is $F_{L,local}$ = 0.38 N when the $f/c = 0.7$. The experimental force measurements found herein show that when using a DC voltage input signal the F_{blk} is bigger than the $F_{L,local}$ when $V_{in} \leq 0$ V. Meanwhile, the dynamic signals produce F_{blk} values in the range of 0.35 and 0.38 N, with the exception at 0.5 Hz, which gives a F_{blk} = 0.41 N. Implying that at driving frequencies > 0.5 Hz the F_{blk} may not overcome the $F_{L,local}$.

5. Summary

This paper presents the first important step towards using TEF technology based on piezoelectric bender actuators. To achieve this goal, this study firstly performs 2D aerodynamic simulations using XFoil on an RG-14 aerofoil with TEFs. Aerodynamic loads are then calculated at the maximum lift coefficient $C_{L,max}$ for different flap-to-chord ratios f/c. It was found that the largest force on the TEF $F_{L,local}$ = 0.39 N and occurred at $f/c = 0.7$.

Afterwards, piezoelectric actuators are characterised for their deflection and force. The total deflection produced by a piezoelectric actuator is important to have a larger flap angle. Meanwhile, the force produced by the actuator is important to overcome aerodynamic forces. Deflection results using constant signals, lead to maximum flap angles of $\beta \pm 3°$, though some drifting is observed. On the other hand, dynamic signals produced overall smaller flap angles and this decreases with increasing signal frequency. Maximum flap angles of $\beta = 2.3°$ and $\beta = -3.2°$ were obtained at 1 Hz. It was also found that hysteresis increased with signal amplitude and frequency. Furthermore, force measurements using static signals have a maximum $F_{blk} = 0.52$ N when fully deflected. Whilst, force measurements using dynamic signals result in smaller forces overall. The maximum F_{blk} is 0.41 N, which is achieved at 0.5 Hz and the smallest F_{blk} is 0.35 N at 15 and 20 Hz.

Experimental force measurements show that for a TEF with $f/c = 0.7$, the piezoelectric actuator overcomes the aerodynamic forces using a static signal. However, the actuator may not be able to overcome the estimated aerodynamic forces when driven with a dynamic signal. Nonetheless, it must be noted that the aerodynamic forces calculated are for large angles of attack and when equipped on a WT, the piezoelectric benders will likely operate at angles of attack smaller than this, meaning that a design with a $f/c = 0.7$ is still possible as long as the angles of attack remain small.

Future work will focus on building a small-scale WT with TEF technology. Experimental results of this study provide crucial information for future WT experiments by building look-up tables to estimate the TEF angle based on the induced voltage signal by the signal generator and the piezo driver.

References

[1] Awada A, Younes R and Ilinca A. 2021. *Energies* **14** 3058
[2] Bak C, Gaunaa M, Andersen P B, Buhl T, Hansen P and Clemmensen K. 2007. *45th AIAA Aerospace Sciences Meeting and Exhibit* p.1016
[3] Barlas T K and van Kuik G AM. 2010. *Progress in Aerospace Sciences* **46** 1 1–27
[4] Barlas T K and Madsen H A. 2015 *International Conference on Adaptive Structures and Technologies* **26** 22
[5] Barlas T, Pettas V, Gertz D and Madsen H A. 2016. *J. Phys.:Conf.Ser.* **753** 042001
[6] Berg J C, Resor B R, Paquette J A and White J R. 2014. Technical Report, Sandia National Lab.
[7] Bilgen O, Kochersberger K B and Inman D J. 2009. *50th AIAA Structures, Structural Dynamics, and Materials Conference* 2009-2133
[8] Buhl T, Bak C, Gaunna M and Andersen P B. 2007. *European Wind Energy Conference and Exhibition* European Wind Energy Association (EWEA) 20-23.
[9] Cai X, Wang Y, Xu B and Feng J. 2020. *Journal of Marine Science and Engineering* **8** (2) 72
[10] Castaignet D, Barlas T, Buhl T, Poulsen N K, Wedel-Heinen J J, Olesen N A, Bak C, Kim T. 2014. *Wind Energy* **17** (4) 549-564
[11] Chopra I. 2002. *AIAA* **40** (11) 2145-2187.
[12] Gomez Gonzalez A, Enevoldsen P B, Barlas A and Madsen H A. 2021. *Wind Energy Science* **6** (1) 33-43.
[13] Hansen M O and Madsen H. 2011. *Review paper on wind turbine aerodynamics* 114001
[14] Hulskamp A, Van Wingerden J, Barlas T, Champliaud H, Van Kuik G, Bersee H E and Verhaegen M. 2011. *Wind Energy* **14** (3) 339-354.
[15] Li H, Shao M, Guo L and An D. 2018.*J. Phys.:Conf.Ser.* **399** 012031
[16] Lodeiro M J, Stewart M and Cain M G. 2005. *Displacement and Blocking Force Measurements of Piezoelectric Macroactuators* National Physical Laboratory (NPL)
[17] Mehta M, Zaaijer M and von Terzi D. 2024. *Wind Energy Science* **9** 141-163
[18] Nanos, EM and Kheirallah, N and Campagnolo, F and Bottasso, CL. 2018 *J. Phys.:Conf.Ser.* **1037** 052016
[19] Porté-Agel F, Bastankhah M and Shamsoddin S. 2020. *Boundary-layer meteorology* **174** 1 1–59
[20] Rios S A and Fleming A J. 2015. *Sensors and Actuators A: Physical* **224** 106-110
[21] Seethaler R, Mansour S P, Ruppert M G and Fleming A J. 2022. *Sensors and Actuators A: Physical* **335** 113384
[22] Shields M, Beiter P, Nunemaker J, Cooperman A and Duffy P. 2021. *Applied Energy* **298** 117189
[23] Selig M S. 1997. *Summary of low speed airfoil data Vol. 3.* SoarTech Publications
[24] van Wingerden J W, Hulskamp A W, Barlas T, Marrant B, van Kuik G AM, Molenaar D and Verhaegen M. 2008. *Wind Energy* **11** 265-280